11th Australasian Fluid Mechanics Conference
University of Tasmania, Hobart, Australia
14-18 December 1992

MEASURING THE EFFECT ON DRAG PRODUCED BY NOSE BLUNTNESS ON A CONE IN HYPERVELOCITY FLOW

L.M. PORTER, D.J. MEE and J.M. SIMMONS

Department of Mechanical Engineering
University of Queensland
QLD 4072, AUSTRALIA

ABSTRACT

Presented in this paper is a preliminary investigation into the effect of nose bluntness on the drag of a conical body in hypersonic flows at Mach numbers above 5 and velocities above 5 kms^{-1}. Experiments have been performed in the T4 hypersonic shock tunnel facility. Since the test time in this facility is of the order of 1 ms, conventional drag measurement techniques can not be used successfully. The new drag measurement technique designed and developed by Sanderson and Simmons (1991) especially for use in short flow duration hypervelocity shock tunnel facilities has been used.

1 INTRODUCTION

The past decade has seen a renewed interest in the development of hypersonic vehicles. A number of different concepts have emerged for the design and application of such vehicles but one issue common to them all is the problem associated with the choice of nose geometry. This is also an issue in the design of an axisymmetric scramjet being proposed as the propulsion system for a disposable launch vehicle where the forebody of the centrebody of the scramjet will be conical. Ideally, in each instance a sharp nose would be used to reduce the pressure drag. However, a pointed slender nose is difficult to cool and does not offer the capability to carry large payloads. These practical limitations have motivated research into the aerodynamic characteristics of a blunted cone. The blunted cone simulates the nose geometry of interest while at the same time may be analysed using simple models. Research into nose cones in subsonic and low supersonic flight regimes is quite extensive but at hypersonic (Mach number greater than 5) and hypervelocity (flight speed greater than 5 kms^{-1}) conditions this is not the case.

The drag force is a fundamental parameter in the design of any flight vehicle but its measurement in hypersonic impulse facilities is inhibited by the very short test times involved. If a conventional force balance or accelerometer balance were to be used to measure drag then the time for a stress wave to traverse a test model would be required to be two orders of magnitude less than the characteristic wind tunnel test time. For an aluminium or steel test model in which the speed of a one-dimensional elastic stress wave is approximately 5 kms^{-1} this requirement would give a maximum model size of 50 mm in a facility having a test time of 1 ms. This is impractical. In order to measure the drag on a larger model in the shorter test time flows the flexibility of the model becomes quite significant and the passage of stress waves within the model needs to be considered. A novel technique for drag measurement in hypersonic impulse facilities has been developed by Sanderson and Simmons (1991). This technique takes into account the distributed mass effects and depends on the interpretation of the transient stress waves propagating within the model and its supporting structure.

The aims of this investigation were twofold. This was the first time the technique had been used in an experimental program. Thus, it was intended to prove through this work that this newly developed technique could be relied upon to provide accurate and reliable measurements of drag. The second aim was to obtain a preliminary measurement of the influence of nose bluntness on the drag on a slender cone. It is envisaged that once having shown that the technique can be used to detect small changes in drag on a cone a more comprehensive investigation into nose bluntness effects can be conducted.

2 EXPERIMENTS

2.1 Facility

The experiments were performed in the T4 free piston driven shock tunnel facility (Stalker and Morgan, 1988). A contoured axisymmetric Mach 5 nozzle was used to expand the gas from the stagnation region to the appropriate test conditions. The nozzle exit plane was 265 mm in diameter and the nozzle throat diameter was 25 mm. The tunnel was operated in a tailored mode so that the static pressure and enthalpy would be constant throughout the flow test time. The results to be presented here were performed in a test gas of air with a freestream Mach number of 5.2. The test gas was at a nominal stagnation enthalpy of 14 MJ/kg and a static pressure of 16 kPa. This condition corresponds to a flight speed of approximately 5.3 kms^{-1}.

2.2 Drag Measurement Technique

The model is attached to a "sting" in the form of a slender elastic bar (see Figure 1). The sting is suspended by vertical threads to allow free movement in the axial direction. Strain gauges located on the sting record the passage of stress waves resulting from the impulsively applied drag force as they are transmitted from the model into the sting.

The dynamic behaviour of the model/sting combination may be modelled as a time-invariant, causal, linear system described by the convolution integral,

$$y(t) = \int_0^t g(t - \tau)\, u(\tau)\, d\tau \qquad (1)$$

where u(t) is the single input to the system, y(t) is the resulting output and g(t) is the unit impulse response function. The unit impulse response function is the response of a system to an impulsive force acting over a very short time (in the limit as time goes to zero), but with a time integral which is finite. Knowing the response of the system to a unit impulsive force it is possible to determine the response of the system to excitation by any arbitrary force via Equation 1. Alternatively, and what is done here, y(t) is obtained from the strain gauge output and a numerical deconvolution process is performed to obtain u(t), the time-history of drag applied to the model.

The unit impulse response function may be obtained numerically from a dynamic finite element program. It has been demonstrated (Simmons et al., 1992) that the technique is insenstive to small changes in the impulse response and that

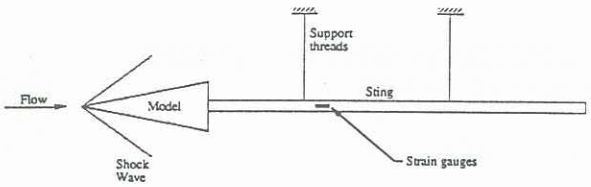

Figure 1. Drag balance configuration.

the unit impulse response function is in turn relatively insensitive to the loading distribution, which will change with varying nose bluntness. The unit impulse response determined for the sharp cone has thus been used in the numerical deconvolution to obtain the drag for all the tests. A complete description of the drag measurement technique is given by Sanderson and Simmons (1991).

2.3 Variable Nose Bluntness Slender Cone Model

Figure 2 shows a diagram of the model/sting arrangement with the finite element mesh used to calculate the unit impulse response function superimposed.

Experiments were performed on a 5° semi-vertex angle aluminium cone of length 571.5 mm. A total of 11 variable nose tips was used ranging in nose radius from 0.2 mm to 18.0 mm in steps of 1.8 mm. These correspond to bluntness ratios of 0.004 to 0.36 where the bluntness ratio is the ratio of the nose radius to the cone base radius. As the nose bluntness is increased, the length of the cone decreases as the base area is kept constant.

Theoretical analysis of a distributed mass model of the model/sting system as performed by Sanderson and Simmons (1991) shows that the mechanical time constant is proportional to the mass of the model. In order that the mechanical time constant of the drag force balance be kept small so that a measurement may be obtained in the small test times, the base area of the cone model was hollowed out to reduce the mass of the cone by almost 50%. Choice of model and sting materials was also dictated by the system time constant (Sanderson and Simmons, 1991). The resulting mechanical time constant of the system was 500 μsec.

Behind the base of the cone there was a PVC buffer to stop motion of the freely suspended model after the test flow. Removing the mass from the cone base served the additional function of ensuring that the pressure in the cavity between the cone and the PVC buffer was negligible by providing a large volume for gas to fill. The base pressure was monitored throughout the tests and the results confirmed this supposition.

The sting had a length of 2.5 m and was constructed from brass tubing of 34.92 mm outside diameter and 1.63 mm wall thickness, making its bending stiffness high. The sting length was chosen so that interference from the stress wave reflected from the end of the sting would not occur during the flow test time. As the speed of propagation of stress waves in brass is 3.600 kms^{-1} a sting length of 2.5 m allowed a test time of 1.3 ms. This estimate of test time takes into account the positioning of the strain gauges 300 mm from the model/sting interface (Figure 1).

2.4 Instrumentation

Kulite UHP-5000-060 semi-conductor strain gauges were used to measure the system output y(t). These gauges have a gauge factor of 155 but they are highly temperature sensitive. This made it necessary to use a modified Wheatstone bridge circuit to compensate the gauge output signals against undesirable temperature effects. Four strain gauges were used. Two gauges were attached to a separate piece of the sting material and placed near the sting so that they saw the same thermal environment but no mechanical strain. The two strain measuring gauges were arranged so that the circuit was sensitive only to axial loads. This was achieved by aligning the gauges in the axial direction and locating them along the neutral axis of bending of the sting so as to eliminate any possible bending effects created by the two wire support system of the sting (Figure 1).

The experiments were conducted in two stages. The first stage was to establish the flow condition and its repeatability. To do this centreline measurements of the static and Pitot pressures in the test flow were obtained. Measuring the drag on the cone model for various nose bluntnesses comprised the second stage of the experiments. Throughout these experiments Pitot pressure measurements were obtained to monitor the test flow properties from one shot to the next. Measurements of the pressure in the base area of the cone were also obtained. Additional instrumentation consisted of the measurement of the shock speeds in the shock tube and stagnation pressures. This is standard procedure as it is these quantities which are used to determine the conditions of the test gas.

3 RESULTS AND DISCUSSION

3.1 Test Flow Conditions

The conditions in the test section were numerically determined using ESTC (McIntosh, 1968) and NENZF (Lordi et al., 1966). The shock speed in the shock tube and the stagnation pressure were measured and used as inputs to ESTC to determine the temperature of the test gas in the stagnation region after shock reflection. The test gas undergoes a steady expansion from the stagnation region to the test flow properties at the exit plane of the nozzle. NENZF is a one-dimensional non-equilibrium code which predicts the properties of the test gas at the exit plane of the nozzle given the stagnation pressure and temperature. The test flow properties thus calculated are shown in Table I.

Measurements made of the test section Pitot pressure and static pressure were found to agree well with those predicted by NENZF. Typical Pitot pressure and static pressure traces are given in Figures 3 (a) and (b). The test flow properties were found to be repeatable to within 10%.

3.2 Drag Measurement Results

Figure 4 shows the raw signal output from the semi-conductor strain gauge bridge. Signals from two separate runs at a nose radius of 0.2 mm are shown here to establish the repeatability of the experimental results. It can be seen that the strain gauge measurements of the system output, y(t), were repeatable to better than 1%.

The strain gauge signal was deconvoluted numerically as described in Section 2.2 to obtain the time history of the drag

Figure 2. Finite element model of sharp cone model and sting.

Table I. Properties of test flow.

Stagnation Enthalpy MJ/kg	Mach No.	Static Pressure kPa	Pitot Pressure kPa	Static Temperature K	Flow Velocity km/s	Density kg/m3
14.4	5.2	16	555	1860	4.50	0.02784

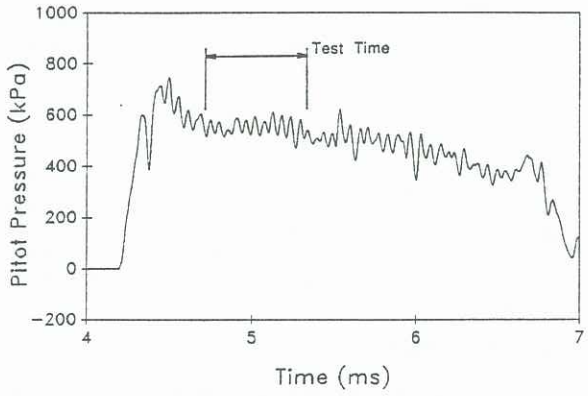

(a)

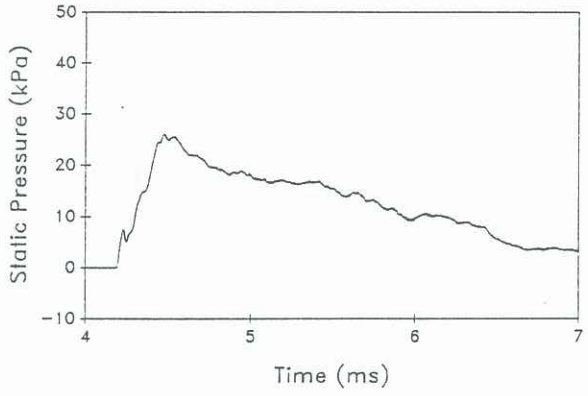

(b)

Figure 3. (a) Measured Pitot pressure and (b) measured static pressure.

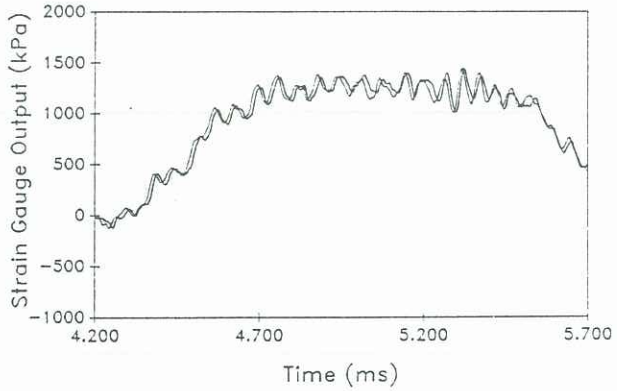

Figure 4. Signal output from strain gauge bridge (converted to stress) for two separate runs for a nose radius of 0.2 mm.

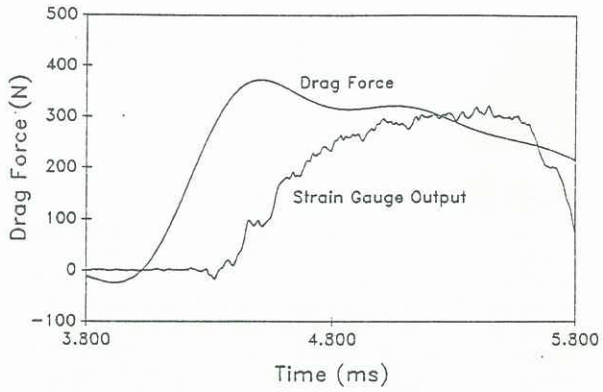

Figure 5. Comparison between signal from strain gauge bridge before (raw signal) and after (drag force) deconvolution for a nose of 10.8 mm.

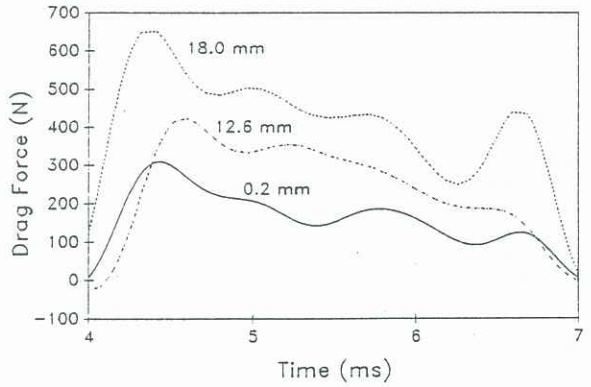

Figure 6. Comparison of the drag force time histories for cones having nose radii of 0.2 mm, 12.6 mm and 18.0 mm.

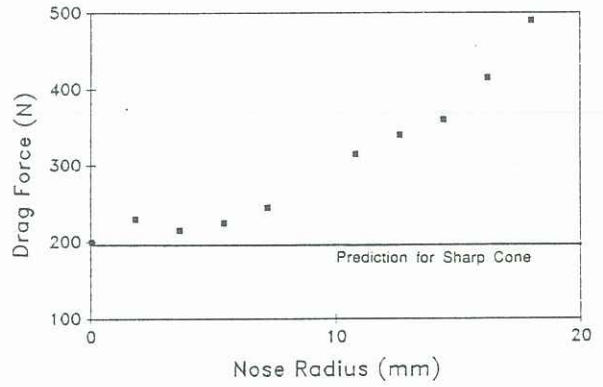

Figure 7. Drag force versus nose radius.

on the model. This drag measurement technique is inherently noisy as the deconvolution process tends to amplify any noise present in the original output signal, y(t). The strain gauge output signal itself is noisy as a result of the stress wave propagation within the model and sting. It was thus necessary to pass all the drag measurements resulting from the numerical deconvolution process through a 2 kHz, 6 pole Butterworth low-pass digital filter.

Figure 5 shows the measured drag in its time-averaged form for a nose radius of 10.8 mm in comparison with its corresponding strain gauge output signal before deconvolution. The time during which the static pressure is steady to within 10% variation (Figure 3) indicates the time of the flow in which the test flow conditions are deemed to be steady. This test time may be identified by the regions of steady drag in the plots of the time history of the drag force

acting on the model (Figures 5 and 6). Figure 6 gives a comparison between the drag measured for the three different nose radii of 0.2 mm, 12.6 mm and 18.0 mm.

Comparison between the static pressure traces (Figure 3) and the drag force traces (Figures 5 and 6) show that the drop in the drag force beyond the test flow time seems to follow the drop in the static pressure after the test time. This indicates that the drag measurement technique is giving faithful measurements of the drag even beyond the test time. The measured drag would be expected to drop with a drop in the static pressure because the drag force on the cone can be split into a pressure drag and a skin friction drag and the pressure drag component, dependent on the flow static pressure, is the larger of the two.

3.3 The Effect of Nose Bluntness on Drag on a Slender Cone

The results from this preliminary investigation into the effects nose bluntness has on cone drag are summarised in Figure 7. It would appear that at the smaller nose bluntnesses the effect on the total drag is relatively minor. The drag shows an increase from the sharp nose value of about 20 % at a nose radius of 7.2 mm (bluntness ratio of 0.144). However, beyond this radius the drag increases more rapidly so that at a nose radius of 18.0 mm (bluntness ratio of 0.36) the value of drag is about 245% greater than for the drag on the sharp cone.

It is uncertain whether the small increase in the value of drag at the 1.8 mm nose radius is due to a real physical effect. It is difficult to draw any conclusions based on this single preliminary result.

A theoretical prediction of the total drag on a sharp cone has been made and is also shown in Figure 7. The pressure drag was predicted using Taylor-Maccoll theory (Taylor and Maccoll, 1932) and found to be 159 N for the case being studied here. An estimate for the skin friction drag on the cone was made based on laminar boundary layer theory (White, 1974) and found to be 36 N. This gives a total drag of 195 N for a sharp, 5° semi-vertex angle and 571.5 mm long cone travelling in air at the condition at which the experiments presented here were conducted. The value of drag measured for the sharp cone was 200 N, thus reinforcing the accuracy of the drag measurement technique used.

4 CONCLUSION

These preliminary results show that the drag measurement technique has been developed to the stage where it can be used as an accurate and reliable research tool. It has been seen that the technique gives a faithful measurement of the time history of drag on a model and can resolve small changes in drag measurement.

The preliminary drag measurement results reveal a steadily increasing effect of nose bluntness on the drag on a cone. The effect at the smaller nose bluntnesses is relatively small, with a 20% increase in drag at a nose bluntness ratio of 0.144. This is encouraging for the design of a hypersonic space plane or a centrebody for an axisymmetric scramjet where a slightly blunted nose is required to reduce stagnation point heating. However, further experiments need to be performed at these smaller nose radii and at a finer resolution to determine the significance, if any, of the jump in drag at the 1.8 mm nose radius.

Further investigation at the larger nose bluntnesses would also be of interest . The results presented here indicate that the drag on a slender cone will continue to increase beyond a nose radius of 18.0 mm. Future experiments will be needed to reveal what effect a further increase in nose radius will have on the drag.

5 REFERENCES

LORDI, J A, MATES, R E and MOSELLE, J R (1966) Computer program for numerical solution of nonequilibrium expansion of reacting gas mixtures. NASA CR-472.

McINTOSH, M K (1968) Computer program for the numerical calculation of frozen and equilibrium conditions in shock tunnels. Dept. of Phys. ANU, Canberra.

SANDERSON, S R and SIMMONS, J M (1991) Drag balance for hypervelocity impulse facilities. AIAA J., 29, 2185-2191.

SIMMONS, J M, DANIEL, W J, MEE, D J and TUTTLE, S L (1992) Force measurement in hypervelocity impulse facilities. Proceedings of Workshop on New Trends in Instrumentation for Hypersonic Research, ONERA Le Fauga - Mauzac, France, 27 April to 1 May.

STALKER, R J and MORGAN, R G (1988) The University of Queensland Free Piston Shock Tunnel T4 - Initial Operation and Preliminary Calibration. NASA CR-181721, Sept. 1988.

TAYLOR, G I and MACCOLL, J W (1932) The air pressure on a cone moving at high speed - I Proc. Royal Soc. (London) Ser. A 139, 278-297.

WHITE, F M (1974) Viscous Fluid Flow. McGraw-Hill, Inc., New York., Inc., New York.